Eur J Nucl Med Mol Imaging (2015) 42:1414–1422
DOI 10.1007/s00259-015-3074-x

ORIGINAL ARTICLE

Quantifying [^{18}F]fluorodeoxyglucose uptake in the arterial wall: the effects of dual time-point imaging and partial volume effect correction

Björn A. Blomberg[1,2] · Arjun Bashyam[3] · Abhinay Ramachandran[3] · Saeid Gholami[3] · Sina Houshmand[3] · Ali Salavati[3] · Tom Werner[3] · Habib Zaidi[4,5] · Abass Alavi[3]

Received: 16 January 2015 / Accepted: 21 April 2015 / Published online: 12 May 2015

Abstract
Purpose The human arterial wall is smaller than the spatial resolution of current positron emission tomographs. Therefore, partial volume effects should be considered when quantifying arterial wall ^{18}F-FDG uptake. We evaluated the impact of a novel method for partial volume effect (PVE) correction with contrast-enhanced CT (CECT) assistance on quantification of arterial wall ^{18}F-FDG uptake at different imaging time-points.
Methods Ten subjects were assessed by CECT imaging and dual time-point PET/CT imaging at approximately 60 and 180 min after ^{18}F-FDG administration. For both time-points, uptake of ^{18}F-FDG was determined in the aortic wall by calculating the blood pool-corrected maximum standardized uptake value ($cSUV_{MAX}$) and $cSUV_{MEAN}$. The PVE-corrected SUV_{MEAN} ($pvcSUV_{MEAN}$) was also calculated using ^{18}F-FDG PET/CT and CECT images. Finally, corresponding target-to-background ratios (TBR) were calculated.
Results At 60 min, $pvcSUV_{MEAN}$ was on average 3.1 times greater than $cSUV_{MAX}$ ($P<.0001$) and 8.5 times greater than $cSUV_{MEAN}$ ($P<.0001$). At 180 min, $pvcSUV_{MEAN}$ was on average 2.6 times greater than $cSUV_{MAX}$ ($P<.0001$) and 6.6 times greater than $cSUV_{MEAN}$ ($P<.0001$).
Conclusion This study demonstrated that CECT-assisted PVE correction significantly influences quantification of arterial wall ^{18}F-FDG uptake. Therefore, partial volume effects should be considered when quantifying arterial wall ^{18}F-FDG uptake with PET.

Keywords PET/CT · [^{18}F]Fluorodeoxyglucose · Arterial wall · Partial volume effect correction · Dual time-point imaging

Introduction

^{18}F-FDG PET/CT is a promising noninvasive imaging technique for assessment of arterial wall inflammation. By targeting arterial plaque glycolysis, a surrogate of arterial inflammation and hypoxia [1, 2], ^{18}F-FDG PET/CT imaging can potentially detect and quantitate arterial inflammation [2, 3], evaluate response to treatment [4, 5], and predict risk for cardiovascular events [6]. Despite several promising studies in the literature [7–10], ^{18}F-FDG PET/CT imaging of arterial inflammation suffers from significant limitations which relates to partial volume effects (PVE) and to the low resolution of PET [11]. PVE is a well-known phenomenon and results in underestimation of the true quantity of radiotracer on PET images. PVE are significant in targeted structures that are two to three times smaller than the spatial resolution of PET [12]. Since the thickness of arterial walls (e.g. 1.5 to 2.5 mm

✉ Abass Alavi
abass.alavi@uphs.upenn.edu

Björn A. Blomberg
b.a.blomberg@umcutrecht.nl

1 Department of Radiology, University Medical Center Utrecht, Heidelberglaan 100, 3584 CX Utrecht, The Netherlands

2 Department of Nuclear Medicine, Odense University Hospital, Odense, Denmark

3 Department of Radiology, Hospital of the University of Pennsylvania, 3400 Spruce Street, Philadelphia, PA 19104, USA

4 Division of Nuclear Medicine and Molecular Imaging, Geneva University Hospital, Geneva, Switzerland

5 Department of Nuclear Medicine and Molecular Imaging, University Medical Center Groningen, University of Groningen, Groningen, Netherlands

for the aorta [13, 14]) is smaller than the spatial resolution of current PET scanners (approximately 5 mm [15]), PVE should be considered in PET imaging of aortic inflammation.

We evaluated the impact of PVE correction with contrast-enhanced CT (CECT) assistance on quantification of arterial wall ^{18}F-FDG uptake at different imaging time-points. In addition, we evaluated the correlations between PVE-corrected measurements and other measurement indices of vessel wall ^{18}F-FDG uptake.

Materials and methods

Subject selection

Subjects were selected from a prospective cohort of patients recruited for the evaluation of lung cancer by multiple time-point ^{18}F-FDG PET/CT imaging. Only subjects with a CECT scan were included in the current study. Patients with tumour involvement near the aorta or other areas of interest were excluded. Ten subjects met the inclusion and exclusion criteria and were included in this study.

Study design

As part of this prospective study, subjects were evaluated by questionnaires, blood pressure measurements, blood analyses, and dual time-point ^{18}F-FDG PET/CT imaging. Subjects also underwent CECT imaging. Questionnaires included questions about prescribed medications, history of cardiovascular disease, and cardiovascular risk factors. Systolic and diastolic blood pressure were obtained from blood pressure measurements. Blood analyses included fasting total serum cholesterol, serum LDL and HDL cholesterols, fasting blood glucose and serum creatinine, and estimated glomerular filtration rate (eGFR) was determined using the Modification of Diet in Renal Disease (MDRD) equation. For each subject, the Framingham risk score was calculated based on age, gender, total serum cholesterol, serum HDL cholesterol, smoking status, systolic blood pressure, and antihypertensive medication status.

^{18}F-FDG PET/CT imaging was performed on an integrated Biograph TruePoint PET/CT scanner (Siemens Healthcare). This scanner combines a lutetium oxyorthosilicate scintillator with a 64-slice CT scanner. Each subject underwent dual time-point PET/CT imaging at 60 and 180 min after intravenous injection of approximately 5.2 MBq of ^{18}F-FDG per kilogram of body weight. ^{18}F-FDG was administered after the subject had fasted for at least 6 h. Before ^{18}F-FDG injection, blood glucose concentration was determined to ensure a value below 11 mmol/L. After injection and between scans, the subject rested in a warm and quiet room. For the 60-min acquisition, the time per bed position was 2 min. For the 180-min acquisition, the time per bed position was 4 min. PET images were acquired from the mid-skull to the mid-thigh and reconstructed in the transverse, coronal and sagittal planes using a point spread function (three iterations, 21 subsets, 4 mm Gaussian filter, 168×168 reconstruction matrix). Corrections were applied for attenuation, scatter, random coincidences and scanner dead time. Low-dose CT imaging was performed for attenuation correction and anatomic orientation. PET data were resampled to the CT voxel grid. No additional rebinning was performed. CECT imaging was performed as part of the routine clinical work-up. PET and CECT images were manually coregistered.

Quantitative image analysis

Quantitative image analysis was performed on a Philips Extended Brilliance Workspace platform. All quantitative analyses were performed on the descending aorta. The following parameters were calculated: area of the arterial lumen (millimetres squared), radius of the arterial lumen (millimetres), arterial wall area (millimetres squared), average arterial wall thickness (millimetres), area of the spillover activity (millimetres squared), average maximum and mean aortic ^{18}F-FDG activity (SUV_{MAX} and SUV_{MEAN}), average blood pool ^{18}F-FDG activity (SUV_{MEAN}), and average background ^{18}F-FDG activity (SUV_{MEAN}). Based on these parameters, the blood pool-corrected SUV_{MAX} and SUV_{MEAN} ($cSUV_{MAX}$ and $cSUV_{MEAN}$) [16], the maximum and mean target-to-background ratio (TBR_{MAX} and TBR_{MEAN}), and the PVE-corrected SUV_{MEAN} ($pvcSUV_{MEAN}$) were calculated.

To determine the area and radius of the arterial lumen, a circular region of interest (ROI) was placed around the contrast-enhanced lumen on every axial slice of the CECT images. On the same images, a second ROI was drawn around the outer perimeter of the arterial wall to determine the area and radius of the descending aorta. Subtracting the luminal area and radius from the area and radius of the descending aorta yielded the arterial wall area and arterial wall thickness. The average arterial wall thickness was calculated as the sum of the arterial wall thickness obtained from all consecutive slices divided by the total number of slices. Based on the parameters obtained from the CECT images, the ROIs were replicated on the ^{18}F-FDG PET/CT images. This replication procedure was performed for every slice. On every slice, a third ROI was drawn to determine the area of spillover activity. The radius of the third ROI was equal to the radius of the second ROI plus the average arterial wall thickness. Per ROI, the maximum and mean ^{18}F-FDG activity concentration (becquerels per millilitre) was determined and recalculated as the SUV_{MAX} and SUV_{MEAN} corrected for radiotracer decay and body weight (kilograms) (Eq. 1). The SUV_{MAX} and SUV_{MEAN} of consecutive slices were summed and divided by the number of slices, resulting in a single average SUV_{MAX} and SUV_{MEAN} value for each subject. Subsequently, the

average values were corrected for blood pool ^{18}F-FDG activity by subtracting the blood pool SUV_{MEAN} to give $cSUV_{MAX}$ and $cSUV_{MEAN}$ [16]. The blood pool SUV_{MEAN} was determined in the superior vena cava by placing a single circular ROI of 100 mm^2 to reduce spillover activity from the vessel wall and other adjacent ^{18}F-FDG-avid structures. The TBR_{MAX} and TBR_{MEAN} were calculated by dividing the average SUV_{MAX} and SUV_{MEAN} by the blood pool SUV_{MEAN}. The background SUV_{MEAN} was determined in the centre of the left psoas major muscle at the level of the iliac crest by placing a single circular ROI of 100 mm^2 to reduce spillover activity from adjacent ^{18}F-FDG-avid structures. After calculating the background activity (Eq. 2), spillover activity (Eq. 3) and blood pool activity (Eq. 4), $pvcSUV_{MEAN}$ was calculated (Eq. 5). All activities (becquerels) were converted to SUV (grams per millilitre) using Eq. 1. Quantitative image analysis is summarized in Fig. 1.

$$\text{Bodyweight corrected SUV}\left(\text{g}/\text{mL}\right) = \frac{\text{Activity concentration}\left(\text{Bq}/\text{mL}\right)\cdot\text{decay correction factor}\cdot\text{bodyweight (g)}}{\text{Injected dosage (Bq)}} \quad (1)$$

$$\text{Background activity(Bq)} = \text{mean background activity}\left(\text{Bq}/\text{mL}\right)\cdot(\text{spillover area}-\text{arterial wall area}-\text{arterial lumen})\left(\text{mm}^2\right)\cdot\text{slice thickness(mm)} \quad (2)$$

$$\text{Spillover activity(Bq)} = \text{mean spillover activity}\left(\text{Bq}/\text{mL}\right)\cdot\text{spillover area}\left(\text{mm}^2\right)\cdot\text{slice thickness (mm)} \quad (3)$$

$$\text{Blood pool activity(Bq)} = \text{mean blood pool activity}\left(\text{Bq}/\text{mL}\right)\cdot\text{arterial lumen}\left(\text{mm}^2\right)\cdot\text{slice thickness(mm)} \quad (4)$$

$$\text{Partial volume corrected mean arterial wall activity concentration(Bq)} = \frac{\text{Spillover activity (Bq)}-\text{blood pool activity(Bq)}-\text{background activity(Bq)}}{\text{Arterial wall area(mm}^2)\cdot\text{slice thickness (mm)}} \quad (5)$$

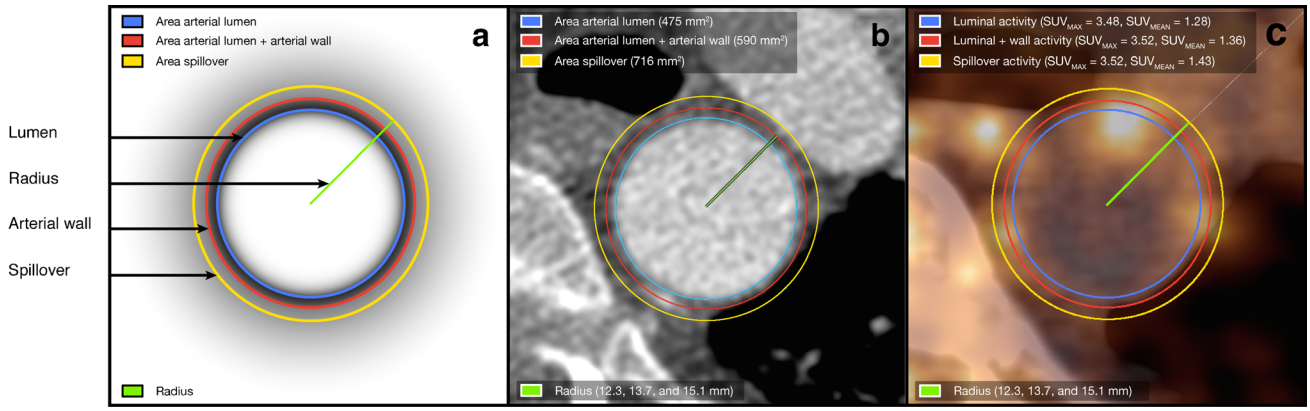

Fig. 1 Placement of regions of interest (ROI) around the arterial lumen (*blue line*), vessel wall (*red line*), and spillover area (*yellow line*) on (**a**) schematic, (**b**) contrast-enhanced CT image, and (**c**) superimposed ^{18}F-FDG PET/CT image. **b** First, the area of the arterial lumen (*blue* ROI) is determined on the contrast-enhanced CT image. On the same images, the area of the aorta (*red* ROI) is determined. Subtracting the luminal area (*blue*) from the aortic area (*red*) yields the arterial wall area. Subtracting their radiuses yields the arterial wall thickness. **c** Based on the area, arterial wall thickness and the radiuses, the blue and red ROIs are replicated on the ^{18}F-FDG PET/CT image. Toward the outside of the artery, at 1.4 mm (arterial wall thickness) from the lateral border of the arterial wall, a spillover region of interest (*yellow*) is drawn to determine the spillover activity. Subtracting the blood pool activity (0.89×475=423) and background activity (0.90×(716−590)=113) from the spillover activity (1.43×716=1,024), and dividing this number by the arterial wall area (590−475=115), results in the partial volume-corrected SUV_{MEAN}: $pvcSUV_{MEAN}$=[1,024−(423+113)]/115=4.24 g/mL. This value is 1.6 and 9.0 times greater than the blood pool-corrected SUV_{MAX} ($cSUV_{MAX}$=3.52−0.89=2.63 g/mL) and SUV_{MEAN} ($cSUV_{MEAN}$=1.36−0.89=0.47 g/mL), respectively. Note that the blood pool (SUV_{MEAN} 0.89 g/mL) and background activity (SUV_{MEAN} 0.90 g/mL) were determined in areas with minimal spillover activity from adjacent structures (i.e. the superior vena cava and the left psoas muscle, respectively)

Table 1 Subject demographics

Characteristic	Value
Age (years), mean (95 % confidence interval)	66.3 (63.3 to 70.0)
Male gender, %	90
Active smoking, %	80
Pack-years, median [25th to 75rh percentiles]	55 [35 to 84.7]
Blood pressure (mmHg), mean (95 % confidence interval)	
Systolic	138.8 (125.2 to 152.6)
Diastolic	77.2 (68.2 to 86.1)
Body mass index (kg/m^2), mean (95 % confidence interval)	23.7 (20.5 to 27.2)
Diabetes mellitus, %	10
Cholesterol (mmol/L), mean (95 % confidence interval)	
Total	4.1 (3.6 to 4.5)
LDL	2.4 (2.0 to 2.8)
HDL	1.2 (1.0 to 1.4)
Triglycerides (mmol/L), mean (95 % confidence interval)	1.0 (0.8 to 1.1)
Blood glucose (mmol/L), mean (95 % confidence interval)	5.6 (5.3 to 5.9)
Creatinine (μmol/L), mean (95 % confidence interval)	70.5 (60.5 to 81.1)
MDRD-eGFR (mL/min/1.73 m^2), mean (95 % confidence interval)	88.6 (78.2 to 100.3)
Medication, %	
Lipid-lowering drugs	50
Antihypertensive drugs	60
Framingham risk score (%), median [25th to 75rh percentiles]	14.5 [8.5 to 21.8]

MDRD-eGFR estimated glomerular filtration rate determined using the Modification of Diet in Renal Disease equation

The 95 % confidence intervals were determined by a bootstrap of 2,000 samples

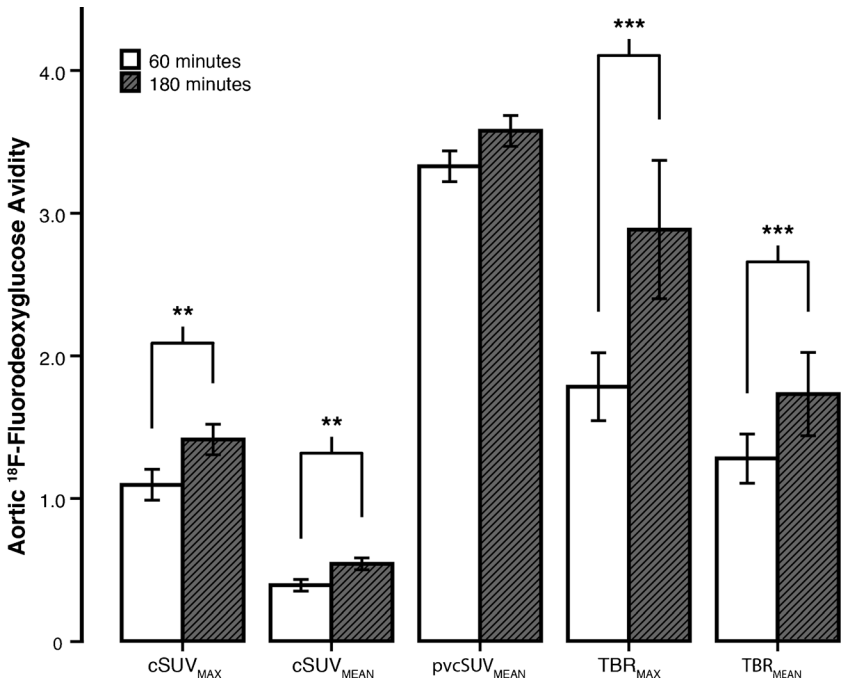

Fig. 2 Aortic ^{18}F-FDG activity at 60 and 180 min after ^{18}F-FDG administration. The blood pool-corrected SUV_{MAX} ($cSUV_{MAX}$), the blood pool-corrected SUV_{MEAN} ($cSUV_{MEAN}$), and the corresponding target-to-background ratios (TBR) significantly increased with time. The partial volume-corrected SUV_{MEAN} ($pvcSUV_{MEAN}$) did not vary with time. At 60 min, the partial volume-corrected SUV_{MEAN} was on average 3.1 times greater than the $cSUV_{MAX}$ ($P<.0001$) and 8.5 times greater than the $cSUV_{MEAN}$ ($P<.0001$). At 180 min, the partial volume-corrected SUV_{MEAN} was on average 2.6 times greater than the $cSUV_{MAX}$ ($P<.0001$) and 6.6 times greater than the $cSUV_{MEAN}$ ($P<.0001$). *Error bars* 95 % confidence interval of the $_{MEAN}$. **$P<.01$, *** $P<.001$, paired Student's *t* test

Intrarater agreement

Intrarater agreement in determining arterial wall thickness on CECT images was assessed in five randomly selected patients 2 months after the initial analysis. Raters were masked from the results of the initial analysis. Interrater agreement was not determined.

Statistical analyses

Subject demographics are summarized as descriptive statistics. Arterial ^{18}F-FDG uptake, quantified as $cSUV_{MAX}$, $cSUV_{MEAN}$, $pvcSUV_{MEAN}$, TBR_{MAX} and TBR_{MEAN}, are summarized and compared using the paired Student's *t* test. Differences in arterial ^{18}F-FDG uptake as a function of the PET acquisition time-point was also evaluated using the paired Student's *t* test. The linearity of the correlation between $pvcSUV_{MEAN}$ and $cSUV_{MAX}$, $cSUV_{MEAN}$, TBR_{MAX} and TBR_{MEAN} was evaluated in terms of Pearson's correlation coefficient (*r*). Intrarater agreement in determining arterial wall thickness was evaluated in terms of the intraclass correlation coefficients (ICC; two-way random effects model assessing absolute agreement of single measures) as well as 95 % limits of agreement according to the method of Bland and Altman [17]. A two-tailed *P* value less than .05 was regarded as statistically significant. The *P* values and 95% confidence intervals were determined using a bootstrap of 2,000 samples. Statistical analyses were performed by IBM SPSS Statistics version 21.

Table 2 Quantitative analysis

	Mean	95 % confidence interval	*p* value
Aortic wall thickness (mm)			
60 min	1.88	1.80 to 1.97	.903
180 min	1.89	1.80 to 1.98	
Background SUV_{MEAN} (g/mL)			
60 min	1.20	0.93 to 1.60	.079
180 min	0.73	0.62 to 0.84	
Blood pool SUV_{MEAN} (g/mL)			
60 min	1.40	1.26 to 1.56	<.0001
180 min	0.77	0.67 to 0.87	
$cSUV_{MAX}$ (g/mL)			
60 min	1.10	0.96 to 1.28	.013
180 min	1.41	1.25 to 1.58	
$cSUV_{MEAN}$ (g/mL)			
60 min	0.39	0.31 to 0.48	.008
180 min	0.54	0.47 to 0.61	
TBR_{MAX}			
60 min	1.78	1.71 to 1.86	.001
180 min	2.88	2.64 to 3.15	
TBR_{MEAN}			
60 min	1.28	1.23 to 1.34	.020
180 min	1.73	1.60 to 1.89	
$pvcSUV_{MEAN}$ (g/mL)			
60 min	3.33	2.89 to 3.75	.092
180 min	3.58	3.06 to 4.08	

p values and 95 % confidence intervals were determined by a bootstrap of 2,000 samples

SUV standardized uptake value, $cSUV_{MEAN}$ blood pool-corrected SUV_{MEAN}, $cSUV_{MAX}$ blood pool-corrected SUV_{MAX}, *TBR* target-to-background ratio, $pvcSUV_{MEAN}$ partial volume-corrected SUV_{MEAN}

Results

Ten subjects at intermediate cardiovascular risk (median Framingham risk score of 14.5 % in 10 years) underwent PET/CT imaging at 65 min (95 % CI 62 to 68 min) and 184 min (95 % CI 181 to 187 min) after ^{18}F-FDG administration (Table 1). Blood pool SUV_{MEAN} significantly decreased with time (*P*<.0001), whereas $cSUV_{MAX}$, $cSUV_{MEAN}$, TBR_{MAX} and TBR_{MEAN} significantly increased with time (*P*=.013, *P*<.01, *P*<.005 and *P*=.020, respectively; Fig. 2). Although background SUV_{MEAN} decreased and $pvcSUV_{MEAN}$ increased with time, the changes were not statistically significant (*P*=.079 and *P*=.092, respectively; Table 2).

At 60 min, $pvcSUV_{MEAN}$ was on average 3.1 times greater than $cSUV_{MAX}$ (3.33 g/mL. 95 % CI 2.89 – 3.75, vs. 1.10 g/mL, 95 % CI 0.96 – 1.28; *P*<.0001) and 8.5 times greater than $cSUV_{MEAN}$ (3.33 g/mL, 95 % CI 2.89 – 3.75, vs. 0.39 g/mL, 95 % CI 0.31 – 0.48; *P*<.0001). At 180 min, $pvcSUV_{MEAN}$ was on average 2.6 times greater than $cSUV_{MAX}$ (3.58 g/mL, 95 % CI 3.06 – 4.08, vs. 1.41 g/mL, 95 % CI 1.25 – 1.58; *P*<.0001) and 6.6 times greater than $cSUV_{MEAN}$ (3.33 g/mL, 95 % CI 2.89 – 3.75, vs. 0.54 g/mL, 95 % CI 0.47 – 0.61; *P*<.0001).

At 60 min, both $cSUV_{MAX}$ and $cSUV_{MEAN}$ were linearly correlated with $pvcSUV_{MEAN}$ (*r*=.69, *P*=.027, and *r*=.66, *P*=.027, respectively). At 180 min, only $cSUV_{MEAN}$ was linearly correlated with $pvcSUV_{MEAN}$ (*r*=.88, *P*=.001; Fig. 3). Neither TBR_{MAX} nor TBR_{MEAN} were related to $pvcSUV_{MEAN}$, either at 60 min or at 180 min (Table 3).

Intrarater agreement in determining aortic wall thickness calculated per slice was considered modest as indicated by an ICC of .38 (95 % CI .31 to .45). The intrarater agreement in determining average aortic wall thickness was considered excellent as indicated by an ICC of .98 (95 % CI .81 to 1.00) with narrow 95 % limits of agreement (Fig. 4).

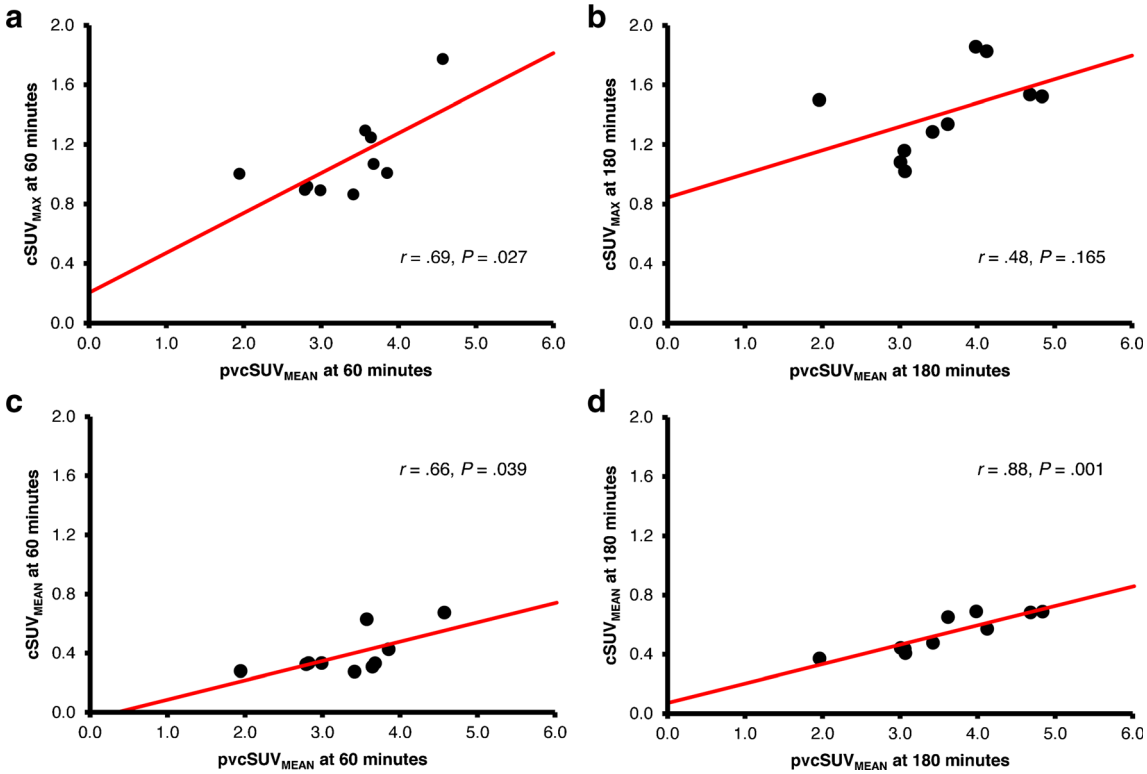

Fig. 3 Correlations between partial volume-corrected SUV_{MEAN} ($pvcSUV_{MEAN}$) and blood pool-corrected SUV_{MAX} ($cSUV_{MAX}$) (**a**, **b**) and between $pvcSUV_{MEAN}$ and blood pool-corrected SUV_{MEAN} ($cSUV_{MEAN}$) (**c**, **d**) at 60 min (**a**, **c**) and 180 min (**b**, **d**) after ^{18}F-FDG administration

Discussion

Our study demonstrated that PVE significantly influences quantification of arterial wall ^{18}F-FDG uptake. Our findings indicate that CECT-assisted measurement of vessel wall $pvcSUV_{MEAN}$ is feasible and the numbers generated are likely to be more accurate than the currently employed ^{18}F-FDG PET indices (SUV_{MEAN}, SUV_{MAX}, $cSUV_{MEAN}$, $cSUV_{MAX}$, TBR_{MEAN}, TBR_{MAX}) at both 60 and 180 min after injection, but the method still needs to be confirmed in phantom studies. The increase in SUV after performing PVE correction is in line with studies investigating the impact of PVE on ^{18}F-FDG uptake in oncological and inflammatory diseases [15, 18, 19]. Nonetheless, among the indices, $cSUV_{MAX}$ and $cSUV_{MEAN}$ at 60 min and $cSUV_{MEAN}$ at 180 min were linearly correlated with $pvcSUV_{MEAN}$. $cSUV_{MEAN}$ at 180 min had the highest linear correlation with PVE-corrected vessel wall ^{18}F-FDG uptake measurements and could be a reliable substitute for $pvcSUV_{MEAN}$.

Table 3 The correlation between partial volume-corrected SUV_{MEAN} and $cSUV_{MAX}$, $cSUV_{MEAN}$, TBR_{MAX}, and TBR_{MEAN}

Time	Pearson's *r*	95 % confidence interval	*p* value
$cSUV_{MAX}$			
60 min	.69	.20 to .95	.027
180 min	.48	.07 to .96	.165
$cSUV_{MEAN}$			
60 min	.66	.19 to .90	.039
180 min	.88	.73 to .99	.001
TBR_{MAX}			
60 min	.15	−.53 to .70	.671
180 min	.20	−.61 to .87	.579
TBR_{MEAN}			
60 min	.30	−.45 to .71	.404
180 min	.51	−.03 to .86	.131

P values and 95 % confidence intervals were determined by a bootstrap of 2,000 samples

SUV standardized uptake value, $cSUV_{MEAN}$ blood pool-corrected SUV_{MEAN}, $cSUV_{MEAN}$ blood pool-corrected SUV_{MAX}, *TBR* target-to-background ratio, $pvcSUV_{MEAN}$ partial volume-corrected SUV_{MEAN}

The impact of PVE on quantification of arterial ^{18}F-FDG uptake has been previously studied. Izquierdo-Garcia et al. evaluated carotid ^{18}F-FDG uptake in seven patients with a recent transient ischaemic attack [20]. Stand-alone PET images were acquired 120 min after injection of 190 MBq of ^{18}F-FDG. In addition, MRI was performed for anatomic orientation. Arterial ^{18}F-FDG uptake was quantified as SUV_{MEAN}, TBR_{MEAN} and ^{18}F-FDG influx rate determined by Patlak analysis. These parameters were corrected for PVE based on the geometric transfer matrix method [21]. PVE correction

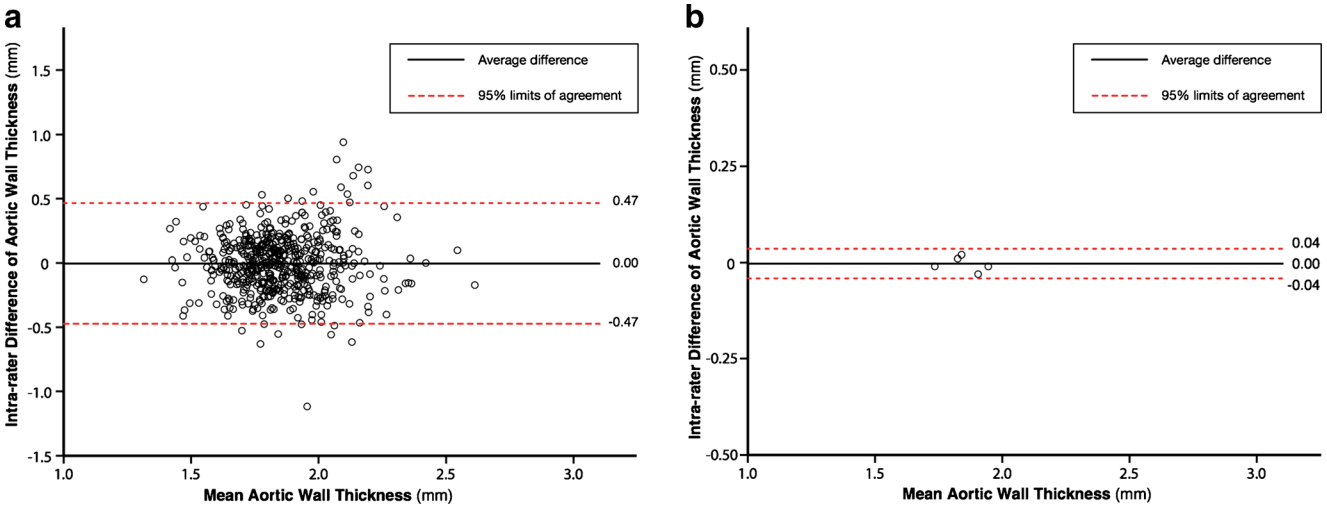

Fig. 4 Intrarater agreement in determining aortic wall thickness as quantified on contrast-enhanced CT images in five patients. **a** Analysis per slice. Although the average intrarater difference is small, intrarater reliability is modest (ICC .38, 95 % CI .31 to .45). **b** Average thickness in each patient. In contrast to the analysis per slice, both agreement and reliability are excellent (ICC .98, 95 % CI .81 to 1.00)

marginally increased the SUV_{MEAN} by 5.7 %. The TBR_{MEAN} and the influx rate did not significantly increase after PVE correction. These findings are in contrast to our study in which PVE correction significantly increased $cSUV_{MEAN}$ by over 800 % and 600 % at 60 and 180 min after ^{18}F-FDG administration, respectively. Despite differences in study methodology (i.e. assessment of the aorta versus carotid artery, CECT-based versus MRI-based PVE correction, and acquisition timepoints of 60 and 180 min versus 120 min), it remains difficult to attribute the discrepant study results to methodological differences only. Differences in PVE correction algorithms are more likely to explain the discrepant results. This hypothesis finds support in a phantom study [22] in which the impact of PVE on quantification of aortic ^{18}F-FDG uptake was evaluated. Based on PET images which simulated the vessels at 60 min after administration of 300 MBq of ^{18}F-FDG, the TBR_{MEAN} and the PVE-corrected TBR_{MEAN} were calculated and compared to the true TBR which was primarily defined in the model. Two methods were used for PVE correction: a method based on arterial wall ^{18}F-FDG activity, arterial wall thickness, and a Gaussian point-spread function, and another method called a geometric transfer matrix method [21]. The Gaussian point-spread function-corrected TBR_{MEAN} was strongly correlated with the true TBR (R^2=.94), but overestimated the true TBR by approximately 60 %. The geometric transfer matrix-corrected TBR_{MEAN} significantly underestimated the true TBR (72 %), but also showed a strong correlation with the true TBR (R^2=.89). On average, Gaussian point-spread function PVE correction increased TBR_{MEAN} by 550 %. On average, geometric transfer matrix-based correction increased TBR_{MEAN} by 193 %. These results suggest that PVE correction algorithms strongly influence quantification of arterial ^{18}F-FDG avidity. Therefore, the discrepant results observed between the studies might be a reflection of the different PVE correction algorithms.

Although our study demonstrated that PVE correction significantly influenced quantification of arterial wall ^{18}F-FDG uptake, it remains to be seen whether correcting for PVE is clinically relevant. In addition, our study was limited by the lack of an accurate reference test of arterial inflammation. Histology of the arterial wall is generally regarded as the reference standard for assessment of arterial inflammation. However, ethical standards prevent collection of arterial specimens in humans. Phantom or animal studies are better suited to this purpose.

So far, only MRI has been successfully used for PVE correction of arterial ^{18}F-FDG uptake [20]. Our study demonstrated the feasibility of CECT imaging for this purpose. Based on arterial wall thickness on CECT, arterial ^{18}F-FDG uptake could be corrected for PVE. Our study demonstrated that the average aortic wall thickness could be determined with excellent intrarater agreement. Previously, we have reported excellent interrater and intrarater agreement in determining aortic wall ^{18}F-FDG uptake indices [16]. Therefore, CECT-based PVE correction of arterial ^{18}F-FDG uptake can be achieved with excellent intrarater agreement. Nonetheless, we acknowledge that manual placement of ROIs for PVE correction can introduce variability among raters. To overcome variability among raters, automated algorithms for placement of ROIs around the aortic wall have been developed [23]. CECT-assisted PVE correction of arterial wall ^{18}F-FDG uptake may benefit from such computerized ROI placement algorithms.

Another potential source of error in our study relates to excessive spill-in activity from adjacent ^{18}F-FDG avid structures. Our study defined background activity by calculating the average ^{18}F-FDG activity in resting skeletal muscle. However, background ^{18}F-FDG activity can exceed that of resting skeletal muscle, for example in tissues such as perivascular fat and bone marrow. This may result in overestimated values of arterial wall ^{18}F-FDG uptake with PVE correction. On the other hand, background ^{18}F-FDG activity can be lower than that of resting skeletal muscle, for example in tissues such as lung. This may result in underestimated values of arterial wall ^{18}F-FDG uptake with PVE correction. More sophisticated PVE correction techniques that take into account variations in background activity may further improve quantification of arterial wall ^{18}F-FDG uptake.

Lastly, patient movement, pulsatile blood flow, and the cardiac and respiratory cycles amplify PVE and may introduce misalignment between PET and coregistered CT images. The impact of these variations on quantification of arterial wall ^{18}F-FDG uptake was not part of the experimental design of this study, and was therefore not investigated. However, considering our observations that PVE correction significantly influenced quantification of arterial wall ^{18}F-FDG uptake, it seems likely that motion compensation could further improve quantification of arterial wall ^{18}F-FDG uptake.

Conclusion

CECT-assisted PVE correction seems to significantly influence quantification of arterial wall ^{18}F-FDG uptake. $pvcSUV_{MEAN}$ did not significantly increase with time. $cSUV_{MEAN}$ and $cSUV_{MAX}$ at 60 min after tracer injection were correlated with $pvcSUV_{MEAN}$, but $cSUV_{MEAN}$ at 180 min had the highest correlation with $pvcSUV_{MEAN}$. Therefore, $cSUV_{MEAN}$ determined at 180 min after injection of ^{18}F-FDG could be a substitute for $pvcSUV_{MEAN}$ as a measure of arterial ^{18}F-FDG uptake.

Compliance with ethical standards

Funding This research was partially supported by a grant from the Department of Veterans Affairs (VISN 4 CPPF grant).

Conflicts of interest None.

Ethical approval This study was approved by the Institutional Review Board of the Philadelphia VA Medical Center and was conducted in accordance with the principles of the Declaration of Helsinki and the Health Insurance Portability and Accountability Act. Written informed consent was obtained from all subjects included in the study.

Financial disclosures The authors have nothing to disclose.

The views expressed in this article are those of the authors and do not necessarily reflect the position or policy of the United States Department of Veterans Affairs or the United States government.

References

1. Folco EJ, Sheikine Y, Rocha VZ, Christen T, Shvartz E, Sukhova GK, et al. Hypoxia but not inflammation augments glucose uptake in human macrophages: implications for imaging atherosclerosis with 18fluorine-labeled 2-deoxy-D-glucose positron emission tomography. J Am Coll Cardiol. 2011;58:603–14. doi:10.1016/j.jacc.2011.03.044.
2. Rudd JH, Warburton EA, Fryer TD, Jones HA, Clark JC, Antoun N, et al. Imaging atherosclerotic plaque inflammation with [18F]-fluorodeoxyglucose positron emission tomography. Circulation. 2002;105:2708–11.
3. Bural GG, Torigian DA, Botvinick E, Houseni M, Basu S, Chen W, et al. A pilot study of changes in (18)F-FDG uptake, calcification and global metabolic activity of the aorta with aging. Hell J Nucl Med. 2009;12:123–8.
4. Tawakol A, Fayad ZA, Mogg R, Alon A, Klimas MT, Dansky H, et al. Intensification of statin therapy results in a rapid reduction in atherosclerotic inflammation: results of a multi-center FDG-PET/CT feasibility study. J Am Coll Cardiol. 2013;62:909–17. doi:10.1016/j.jacc.2013.04.066.
5. Tahara N, Kai H, Ishibashi M, Nakaura H, Kaida H, Baba K, et al. Simvastatin attenuates plaque inflammation: evaluation by fluorodeoxyglucose positron emission tomography. J Am Coll Cardiol. 2006;48:1825–31. doi:10.1016/j.jacc.2006.03.069.
6. Rominger A, Saam T, Wolpers S, Cyran CC, Schmidt M, Foerster S, et al. 18F-FDG PET/CT identifies patients at risk for future vascular events in an otherwise asymptomatic cohort with neoplastic disease. J Nucl Med. 2009;50:1611–20. doi:10.2967/jnumed.109.065151.
7. Bucerius J, Mani V, Moncrieff C, Rudd JH, Machac J, Fuster V, et al. Impact of noninsulin-dependent type 2 diabetes on carotid wall 18F-fluorodeoxyglucose positron emission tomography uptake. J Am Coll Cardiol. 2012;59:2080–8. doi:10.1016/j.jacc.2011.11.069.
8. Rudd JH, Myers KS, Bansilal S, Machac J, Pinto CA, Tong C, et al. Atherosclerosis inflammation imaging with 18F-FDG PET: carotid, iliac, and femoral uptake reproducibility, quantification methods, and recommendations. J Nucl Med. 2008;49:871–8. doi:10.2967/jnumed.107.050294.
9. Kim TN, Kim S, Yang SJ, Yoo HJ, Seo JA, Kim SG, et al. Vascular inflammation in patients with impaired glucose tolerance and type 2 diabetes: analysis with 18F-fluorodeoxyglucose positron emission tomography. Circ Cardiovasc Imaging. 2010;3:142–8. doi:10.1161/CIRCIMAGING.109.888909.
10. Bucerius J, Duivenvoorden R, Mani V, Moncrieff C, Rudd JH, Calcagno C, et al. Prevalence and risk factors of carotid vessel wall inflammation in coronary artery disease patients: FDG-PET and CT imaging study. JACC Cardiovasc Imaging. 2011;4:1195–205. doi:10.1016/j.jcmg.2011.07.008.
11. Menezes LJ, Kotze CW, Hutton BF, Endozo R, Dickson JC, Cullum I, et al. Vascular inflammation imaging with 18F-FDG PET/CT: when to image? J Nucl Med. 2009;50:854–7. doi:10.2967/jnumed.108.061432.
12. Basu S, Zaidi H, Houseni M, Bural G, Udupa J, Acton P, et al. Novel quantitative techniques for assessing regional and global function and structure based on modern imaging modalities: implications for normal variation, aging and diseased states. Semin Nucl Med. 2007;37:223–39. doi:10.1053/j.semnuclmed.2007.01.005.

13. Mensel B, Quadrat A, Schneider T, Kuhn JP, Dorr M, Volzke H, et al. MRI-based determination of reference values of thoracic aortic wall thickness in a general population. Eur Radiol. 2014;24:2038–44. doi:10.1007/s00330-014-3188-8.
14. Shakeri A, Hafez Quran F, Javadrashid R, Abdekarimi MH, Ghojazadeh M, Abolghassemi Fakhree MB. Correlation between aortic wall thickness and coronary artery disease by 64 slice multidetector computed tomography. J Cardiovasc Thorac Res. 2013;5:91–5. doi:10.5681/jcvtr.2013.020.
15. Sanchez-Crespo A, Andreo P, Larsson SA. Positron flight in human tissues and its influence on PET image spatial resolution. Eur J Nucl Med Mol Imaging. 2004;31:44–51. doi:10.1007/s00259-003-1330-y.
16. Blomberg BA, Thomassen A, Takx RA, Hildebrandt MG, Simonsen JA, Buch-Olsen KM, et al. Delayed 18F-fluorodeoxyglucose PET/CT imaging improves quantitation of atherosclerotic plaque inflammation: results from the CAMONA study. J Nucl Cardiol. 2014;21:588–97. doi:10.1007/s12350-014-9884-6.
17. Bland JM, Altman DG. Statistical methods for assessing agreement between two methods of clinical measurement. Lancet. 1986;1:307–10.
18. Salavati A, Borofsky S, Boon-Keng TK, Houshmand S, Khiewvan B, Saboury B, et al. Application of partial volume effect correction and 4D PET in the quantification of FDG avid lung lesions. Mol Imaging Biol. 2015;17:140–8. doi:10.1007/s11307-014-0776-6.
19. Saboury B, Salavati A, Brothers A, Basu S, Kwee TC, Lam MG, et al. FDG PET/CT in Crohn's disease: correlation of quantitative FDG PET/CT parameters with clinical and endoscopic surrogate markers of disease activity. Eur J Nucl Med Mol Imaging. 2014;41:605–14. doi:10.1007/s00259-013-2625-2.
20. Izquierdo-Garcia D, Davies JR, Graves MJ, Rudd JH, Gillard JH, Weissberg PL, et al. Comparison of methods for magnetic resonance-guided [18-F]fluorodeoxyglucose positron emission tomography in human carotid arteries: reproducibility, partial volume correction, and correlation between methods. Stroke J Cereb Circ. 2009;40:86–93. doi:10.1161/STROKEAHA.108.521393.
21. Rousset OG, Ma Y, Evans AC. Correction for partial volume effects in PET: principle and validation. J Nucl Med. 1998;39:904–11.
22. Burg S, Dupas A, Stute S, Dieudonne A, Huet P, Le Guludec D, et al. Partial volume effect estimation and correction in the aortic vascular wall in PET imaging. Phys Med Biol. 2013;58:7527–42. doi:10.1088/0031-9155/58/21/7527.
23. Reeps C, Bundschuh RA, Pellisek J, Herz M, van Marwick S, Schwaiger M, et al. Quantitative assessment of glucose metabolism in the vessel wall of abdominal aortic aneurysms: correlation with histology and role of partial volume correction. Int J Cardiovasc Imaging. 2013;29:505–12. doi:10.1007/s10554-012-0090-9.